Nuclear Engineering and Design 445 (2025) 114529

Contents lists available at ScienceDirect

Nuclear Engineering and Design

journal homepage: www.elsevier.com/locate/nucengdes

Dynamical modeling of the thermal stress in the nozzle corner of reactor pressure vessels for model-based power maneuvering control design

Bálint Pudleiner [a], Tibor Szűcs [a], Tamás Fekete [a], Pal Szentannai [a,b,*]

[a] HUN-REN Centre for Energy Research, Konkoly-Thege rd. 29-33, H-1121 Budapest, Hungary
[b] Department of Energy Engineering, Faculty of Mechanical Engineering, Budapest University of Technology and Economics, Muegyetem rkp. 3, H-1111 Budapest, Hungary

ARTICLE INFO

Keywords:
Load-following operation
Thermal stress
Numerical methods
Life-Time Considering Control (LTCC)
Health-Aware Controller (HAC)

ABSTRACT

Knowledge of the dynamic evolution of thermal stresses in the critical points of nuclear power plants is essential for establishing optimized maneuvering control. It must, namely, balance between power accuracy at the generator side and material fatigue at the reactor side. To set up the mathematical description of the lacking latter side, we aim in the current study to build it in such a form that fits the language of control theory and that of dynamical optimum-seeking procedures. Accordingly, the *transfer function* in the Laplacian space is formulated for the subprocess, the input variable of which is the moderator temperature in the upper plenum, and the output variable is the thermal stress in the nozzle corner. To achieve this, we set up the 3D models of all consecutive subprocesses (fluid dynamics, heat transfer, strength of material), between which back-couplings were, in most cases, reasonably neglected. To make the 3D calculations absolutely reliable, we used two basically different, independent FEM/FVM environments. From this, the *step response function* was gained, from which, by means of curve fitting, the final dynamical model was achieved.

1. Introduction

The primary challenge associated with electrical energy lies in its storage, which remains unresolved in terms of both efficiency and scale. As a result, maintaining a constant equilibrium between real-time consumption and generation is essential. Since influencing the demand side is practically infeasible, and the supply side increasingly includes elements that are not controllable, the burden of maintaining system stability falls entirely on the remaining controllable sources. So, the rise of variable renewable energy sources, coupled with a reduction in easily dispatchable fossil-fueled plants, necessitates that large power-generating units operate in load-following mode (Marusic et al., 2016) – despite these units traditionally being designed for steady-state operation.

Nuclear power plants (NPPs) are prime examples of such systems (Raskovic et al., 2022), where safety, economic efficiency, and environmental impact are of predominant importance. Because of these factors, a critical consideration is whether NPPs can indeed operate in the load-following regime. A massive body of operational experiences confirms that they can, that is, NPPs are able to contribute to climate action (Szentannai and Fekete, 2025). Germany offers a notable case: prior to its political shift in energy strategy, detailed investigations demonstrated that several nuclear units successfully engaged in load-following mode nearly continuously throughout the year, as documented in multiple studies (Ludwig et al., 2010; Grunwald and Caviezel, 2017).

Optimal designing of the controllers of nuclear power plants requires the control oriented model of the plant (Rabie et al., 2024). In the case of its application in the maneuvering regime (Abdulraheem and Korolev, 2021), dynamic modeling of the determining limiting and adverse effect is also essentially needed (Hu et al., 2024; Salman and Gomaa, 2025). A summary of such effects is listed in IAEA (2018), among which thermal load and fatigue appear to be by far the most important ones. Although fuel rods may also be affected in this way, in the current study, we focus on the primary area, the nozzle corner (Liu et al., 2018; Cheng et al., 2023). This is because the reactor pressure vessel is practically not replaceable (Liu et al., 2018), hence its service life time directly determines the technically permissible service life of the entire nuclear power unit (Kondryakov and Kharchenko, 2024). Further, its big size, complex geometry, and thickness claim special attention (Rabazzi et al., 2024), and here, the most vulnerable place is the nozzle ring (Li et al., 2020b). Although the geometry of such junctions is rather complex (Wang et al., 2023), an analytical description of the thermal stresses at the critical points is possible (Dzierwa et al., 2014; Oh et al., 2022), provided that the edge along the hole is

* Corresponding author at: HUN-REN Centre for Energy Research, Konkoly-Thege rd. 29-33, H-1121 Budapest, Hungary.
E-mail address: szentannai.pal@ek.hun-ren.hu (P. Szentannai).

https://doi.org/10.1016/j.nucengdes.2025.114529
Received 16 June 2025; Received in revised form 26 August 2025; Accepted 5 October 2025
Available online 15 October 2025

Nomenclature

Abbreviations	
FEM	finite element method
FVM	finite volume method
PWR	pressurized water reactor
RPV	reactor pressure vessel
Symbols	
c	specific heat capacity (J/kg/K)
$G(s)$	transfer function
h	heat transfer coefficient (W/m^2/K)
p	pressure (Pa)
$\dot{q}$	heat flow rate (W/m^2)
s	argument in the Laplace domain (1/s)
t	time (s)
T	temperature (K)
$\mathbf{T}$	Laplace transform of the temperature
u	velocity (m/s)
Greek letters	
κ	thermal conductivity (W/m/K)
ρ	density (kg/m^3)
σ	thermal stress (MPa)
$\mathbf{\Sigma}$	Laplace transform of the thermal stress
τ	shear stress (MPa)
Subscripts	
ext	external
l	liquid phase
s	solid phase

sharp. Unfortunately, this is not the case in the region investigated in the current study, as pointed out by Trampus (2024).

For modeling fluid dynamics, a widely used methodology is available, which is applied for very diverse purposes; thus, its use for the area investigated by us is not unprecedented. Such a study by Sharabi et al. (2016) published results obtained with a commercial FVM tool. In their work, two well-known turbulence models (k-ϵ and k-ω) were investigated, and no significant differences were found between their results. Similar investigations were conducted for several, but fundamentally comparable reactor pressure vessel geometries by Ayhan and Ergün (2013).

Both of the above-mentioned studies also included 3D calculations of heat transfer between the liquid and the wall in the critical region as a direct consequence of the fluid dynamical results. Furthermore, Sharabi et al. (2016) extended their modeling to thermomechanical processes within the solid wall, however, most studies start only from this point. This latter approach characterizes the majority of analyses, in which both fluid dynamics and the fluid–wall interaction are significantly simplified by applying boundary conditions prescribed by temperatures or heat transfer coefficients.

International literature is dominated by studies of this type since such simplifications omit a computationally very demanding step, and are assumed not to significantly reduce the accuracy of the results. A good example of this approach is provided by Chaudhry et al. (2014), who performed structural integrity calculations for a specific nuclear power plant. Similar methodologies – mainly for the purpose of describing crack propagation in the critical part of the reactor vessel, with particular attention to load-following – have also been applied by several authors (Liu et al., 2020; Li et al., 2020b; Jin et al., 2021; Mohanty et al., 2016).

While describing the behavior of the solid body of the reactor pressure vessel, more precisely, its nozzle corner, the target of the actual investigation must be kept in mind. Namely, in the case of any control actions, the resulting loads can by no means approach the *elastic limit* of the actual material (Liu et al., 2018). Similarly, the phenomenon of *creep* should also be excluded from using the discipline *strength of materials* (Lemaître and Chaboche, 2005). Further, because of the same reason, the actual *stress intensity factor* – as defined by the discipline *fracture mechanics* – cannot reach its critical value (Liu et al., 2021), above which catastrophic crack extension (fracture) occurs (Miedlar et al., 2002; Naweed et al., 2023). Similarly, the mathematical description of *slow crack growth* must also be excluded from the scope of the current investigations (Santucci et al., 2007).

The phenomenon to consider is called *material aging*. About this, two basic directions of the theory are known, summarized by Rodriguez-Reyes et al. (2024) and Ray et al. (1994). Both theories rely on the time function of the stress, which is caused by temperature changes. Exactly this is what happens throughout load variations of the plant, caused by maneuvering control actions.

As visible, determining the thermal stress as a function of time is a key objective. Since it is caused by temperature changes, a simple and computationally efficient approach is to assume it is proportional to the rate of temperature change ($\mathrm{d}T/\mathrm{d}t$). This rather simple approach is widely applied in recent and earlier studies (Rusin et al., 2021; Belkhir et al., 2015), in standards (EN12952-3, 2021), as reviewed in detail by Szentannai and Fekete (2022).

Giving a directly usable support to the apparently high research activities on *nuclear power plant control* was one specific aim of the current research. This observable trend results, namely, in a high number of high impact advanced solutions, especially for PWRs in load-following mode. Many of these reports propose a more sophisticated use of the classical PID controller (Zhou and Tan, 2023; Sun et al., 2021; Abdulraheem and Korolev, 2021; Mousakazemi, 2021; Zeng et al., 2021; Vajpayee et al., 2020). Furthermore, regardless of this, they either apply deterministic theoretical control methods (Sun et al., 2021; Vajpayee et al., 2021; Abdulraheem and Korolev, 2021; Vajpayee et al., 2020), or some outcomes of the intelligence research (Park et al., 2022; Mousakazemi, 2021; Zeng et al., 2021; Elsisi and Abdelfattah, 2020). By using the results of the current report, all these research activities will also be able to involve in their methodologies another essential time-dependent output variable: the thermal stress in the most critical point of the reactor pressure vessel. This is the explicit goal of this paper, which offers a significant improvement against the use of static stress models by means of the proposed dynamical stress model. Its importance is also underlined by the increasingly compelling load-following operation of nuclear power plants.

In this study, we set up the instationary model of the stress in the nozzle corner – in the most critical area of a reactor pressure vessel – as a function of moderator temperature, formulated in such a form that fits the language of control theory. Although suitable dynamical models are available to support model-based load-following control of pressurized water nuclear power units, there is still a lack of models that capture the resulting thermal stresses in the critical points. Consequently, the mathematical representation of one side of the two conflicting requirements associated with load changes is missing, which prevents truly optimal maneuvering. To address this gap, we first set up the 3D model of all phenomena needed for calculating the stress field caused by varying the moderator temperature during a load-changing transient. We then perform dynamical system identification to derive a final representation of this subsystem in the form of a *transfer function*, which is well suited to instationary modeling and hence dynamical optimization. The proposed procedure is demonstrated for a typical nozzle layout, and to ensure the reliability of the 3D calculations, we employed two fundamentally different, independent FEM/FVM environments.

2. Modeled area and modeling tools

2.1. Nozzle corner

Optimal controller design of nuclear power plants in the maneuvering regime also requires adequate dynamical modeling of the most

Table 1
Material properties of the reactor pressure vessel (RPV) and the nozzles.

Yield strength (MPa)	450–490
Young's modulus (GPa)	~ 210
Poisson's ratio (–)	~ 0.3
Density (g/cm^3)	~ 7.85
Coefficient of thermal expansion (1/K)	~ $12 \cdot 10^{-6}$

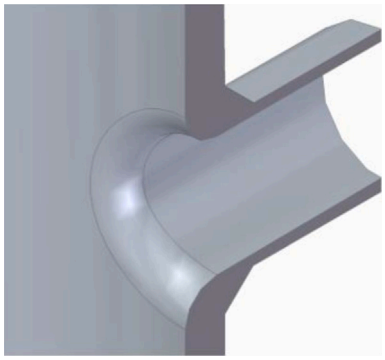

Fig. 1. CAD model of the nozzle corner. (In the specific application case of the procedure, the reactor pressure vessel's internal diameter is 4000 mm, the nozzle's internal diameter is 850 mm, and all further geometric and material data are as per Trampus (2024).).

relevant adverse effect, thermal stresses in the reactor pressure vessel. In this practically non-replaceable component of big size and complex geometry, the most vulnerable place is the nozzle ring (Li et al., 2020a), especially the nozzles at the hot water outlet. This is because higher stresses occur in the wall of the nozzle ring under load than in geometrically undisturbed parts of the reactor pressure vessel. This ring is sufficiently far from the core ring (which surrounds the reactor core), so neutron irradiation is negligible. Therefore, embrittlement processes do not occur here, and material properties can be considered constant during normal operation (Trampus, 2024).

The more specific area investigated in this study is the nozzle corner of one selected power plant type, the details of which, together with the necessary geometric data, were reported by Trampus (2024). According to that paper, the RPV and its nozzles are made of 15Cr2NiMoVA, a low-alloy, high-strength steel, which is commonly used in pressure vessel applications. Its specific material properties are summarized in Table 1. The solid modeling of this part was performed by creating the 3D geometry, the result of which is shown in Fig. 1. The direct application of the current method was done explicitly for this case, characterized by the above geometric and material data. Investigating the effects of changes in any of them is out of the current scope. In the present study, the cladding is not taken into account because its thickness is far below 10% of the wall thickness of the reactor pressure vessel, and in this case, the influence of the cladding on the load behavior is negligible (Jeong et al., 2022).

2.2. Numerical environments

We applied in parallel two different, widely used tools in numerical modeling, OpenFOAM and MSC-Marc, the basic characteristics of which are summarized as follows (Greenshields and Weller, 2022; Ochsner and Ochsner, 2018).

OpenFOAM is an open-source, highly flexible simulation platform originally designed for Computational Fluid Dynamics (CFD), but extended to support structural mechanics, heat transfer, and multi-physics problems as well. MSC-Marc is a commercial software for handling problems such as structural analysis, stress–strain calculations, and thermomechanical coupling. Their differences become evident when comparing solver capabilities, computational performance, and usability.

OpenFOAM provides over 80 built-in solvers and supports user-defined modifications. It is widely used for large-scale CFD problems, such as turbulence modeling and heat transfer, with benchmarks showing scalability up to 100,000 processor cores. Accordingly, it outperforms MSC-Marc in fluid–structure interaction problems requiring high mesh resolution and computational fluid dynamics (CFD) integration. MSC-Marc, in contrast, focuses on non-linear numerical analysis, and its solvers are optimized for industrial applications, achieving solution convergence up to 10×faster than general-purpose open-source numerical tools. Both software packages are systematic numerical methods for solving partial differential equations (PDEs). However, their basic approaches are different, as OpenFOAM is based on the finite volume method (FVM), while MSC-Marc applies the finite element method (FEM).

Another distinction between the two is usability. OpenFOAM operates primarily through a command-line interface, requiring users to write case files and configure solvers manually. In contrast, MSC-Marc provides a graphical user interface (GUI) with integrated pre- and post-processing, significantly reducing setup time.

OpenFOAM, as a free and open-source tool, has a large community with over 20,000 active users and extensive online support. MSC-Marc, as commercial software, requires a license at a markedly high price per seat.

We used the above two essentially different numerical tools throughout the current project to eliminate any numerical-based definite errors in the computational results. The mesh quality metrics we applied throughout our calculations (orthogonality > 0.2, skewness < 0.3) are well within the recommended ranges proposed in the literature. In addition, the number of cells through the wall thickness significantly exceeds the typical minimum of 5–6, and the boundary layer resolution is more than twice the common minimum of 3. These facts indicate low cell distortion, good numerical stability, and strongly suggest that the mesh is adequate and the simulation results are reliable. Further, although we also applied other techniques generally known for single-platform simulations, including grid independence tests, e.g., we believe that the cross-validation via two independent numerical tools expels a much broader range of numerical mistakes, hence this is definitely a rather robust approach.

2.3. Curve fitting

For getting the generally applicable dynamical description of the thermomechanical system in question, fitting a curve to the points resulted from the 3D calculations was needed. The related theory of *system identification* was summarized in the essential book of Ljung (1998), and throughout our calculations, we applied a software package developed and introduced – jointly with others – by Ljung (2024). This is an extension to the basic package of the commercial, matrix-based language and software environment *Matlab*, which we also used for many other purposes throughout the current work, including several calculations, analyses, and visualization of 2D results. We chose this environment because, on the one hand, Matlab is a well-known and extensively applied tool in the worldwide scientific community, and, on the other hand, its decisive algorithms are written by the highest-level professionals in the subject areas.

The *System Identification Toolbox* is capable of creating linear and nonlinear dynamic system models from several types of series of discrete data pairs. Among its offered possibilities, we applied the `tfest` function as this is the one that estimates the best fitting continuous-time transfer function based on the time function achieved from the preceding 3D calculations.

Prerequisites for using this code are to have chosen some properties of the model, such as its being linear, together with the degree of both the nominator and denominator of the transfer function to be estimated in the frequency-domain. We applied graphical comparisons between the original and the estimated system responses to judge the goodness of the identification, including also the above-mentioned decisions.

3. Steps of dynamical modeling

The input variable of the process to be modeled in this study is the moderator's instationary temperature in the upper plenum of the reactor pressure vessel. On the other hand, the output of the current model should be the von Mises thermal stress in the nozzle corner, also as function of time.

From this declaration comes the series of submodels to be elaborated in the upcoming subsections: (i) fluid dynamics, (ii) convective heat transfer between fluid and solid, (iii) thermal conduction within the solid body, and (iv) strength of materials calculation for gaining the field of thermal stresses within the investigated solid. As visible, the calculation method involves several submodels, that is, it is composed of multiple physical fields, the descriptions of which must be coupled. Regarding this, the most complicated case is the heat transfer between two phases, the liquid fluid and the solid wall. For handling it, the applied FEM/FVM tools are well prepared by means of applying the so called *nearest neighbor search*. It simply means that at the closest elements of connecting surfaces, the temperatures are assured to be the same. In the current study, the physical meaning of all other couplings can be considered as purely straightforward effects, that is, here, all feedback effects can be neglected. This is why the current modeling process can be carried out simply stepwise.

In order to make the above outlined modeling procedure usable for dynamical modeling and optimum seeking, the results must be translated into the language of the appropriate disciplines. For this, we applied a step-like function on the input of the above described subprocess, and so the resulting output is the so-called *step response function*, which is a standard representation of any processes in control theory. From this, an easy-to-use description, the *dynamical transfer function* can be gained by curve fitting.

The topic of the rest of this section is a detailed description of the above-mentioned steps, together with their results in the specifically investigated real case.

3.1. Fluid dynamics

Modeling the fluid flow in the investigated region is based on the Navier–Stokes Eq. (1), supplemented by the continuity (2), applied for incompressible fluids:

$$\rho_{\mathrm{l}}\left(\frac{\partial \boldsymbol{u}}{\partial t}+(\boldsymbol{u}\cdot\nabla)\,\boldsymbol{u}\right)=-\nabla \boldsymbol{p}+\nabla\cdot\boldsymbol{\tau}+F_{\mathrm{ext}} \tag{1}$$

$$\nabla\cdot\left(\rho_{\mathrm{l}}\boldsymbol{u}\right)=0 \tag{2}$$

where $\boldsymbol{u}$ is the local fluid velocity vector, ρ is density, $\boldsymbol{p}$ is pressure, $\boldsymbol{\tau}$ is the local shear stress tensor, and F_{ext} summarizes the external forces.

For Newtonian fluids, the stress tensor $\boldsymbol{\tau}$ can be expressed as:

$$\boldsymbol{\tau}=\mu\left(\nabla\boldsymbol{u}+(\nabla\boldsymbol{u})'\right)+\lambda(\nabla\cdot\boldsymbol{u})\bar{\bar{1}} \tag{3}$$

where μ and λ are dynamic and volume viscosity, respectively.

Due to the high flow velocity and geometric variations, the flow is clearly turbulent. Turbulence is modeled using the Reynolds-Averaged Navier–Stokes (RANS) approach, in which any flow variable ψ is decomposed into a mean and a fluctuating component:

$$\psi=\bar{\psi}+\psi^{*} \tag{4}$$

Applying this decomposition introduces the Reynolds stress tensor R_{ij}, accounting for the effect of velocity fluctuations:

$$R_{ij}=-\mu_{\mathrm{T}}\left(\nabla\boldsymbol{u}+(\nabla\boldsymbol{u})'\right)+\frac{2}{3}\rho_{\mathrm{l}}k \tag{5}$$

where μ_{T} is the turbulent (or eddy) viscosity, and k is the turbulent kinetic energy associated with the fluctuating velocity components.

To close the model, two-equation turbulence models are commonly used, such as the k–ϵ and k–ω models. These solve transport equations for k and either its dissipation rate ϵ, or its specific dissipation rate ω. The k–ω SST (Shear Stress Transport) model combines the strengths of both approaches, using k–ω near walls and transitioning to k–ϵ in the free stream.

The turbulent viscosity is then determined from:

$$\mu_{\mathrm{T}}=\rho_{\mathrm{l}}C_{\mu}\frac{k^{2}}{\epsilon} \tag{6}$$

These models are implemented in standard CFD tools such as OpenFOAM, which includes the necessary equations and empirically derived constants.

One example at a selected time instance of the results is depicted in Fig. 2. Based on this, the heat transfer coefficients can already be calculated as well. As visible, next to the wall, the liquid velocity is rather low, and the flow becomes heavily turbulent. Accordingly, the calculated heat transfer coefficient values are significantly higher in the turbulent region.

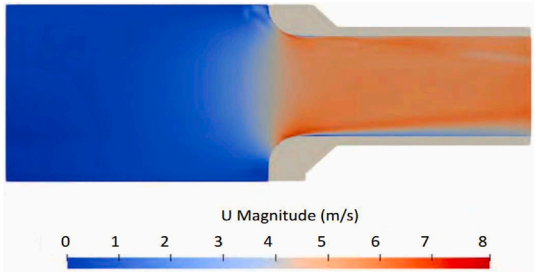

Fig. 2. Velocity field around the nozzle corner 100 s after the initial excitation, as an example of the results of the fluid dynamical investigations.

3.2. Convective heat transfer

The fluid dynamical matters determine the actual conditions of heat transfer between fluids and solids. To describe this latter phenomenon, firstly, the energy equation for the liquid side must be formulated, as follows:

$$\rho_{\mathrm{l}}c_{\mathrm{l}}\frac{\partial T_{\mathrm{l}}}{\partial t}+\rho_{\mathrm{l}}c_{\mathrm{l}}(\boldsymbol{u}\cdot\nabla)\,T_{\mathrm{l}}-\nabla\cdot\left(\kappa_{\mathrm{l}}\nabla T_{\mathrm{l}}\right)=\dot{q}_{\mathrm{l\text{-}s}} \tag{7}$$

The first term on its left-hand side describes the effect caused by the change of the liquid temperature T_{l}, the second one, the convective heat transfer caused by the liquid velocity $\boldsymbol{u}$, and the third one the heat transfer characterized by the liquid's thermal conductivity κ_{l}. On the right-hand side, $\dot{q}_{\mathrm{l\text{-}s}}$ is the heat transfer rate.

The energy equation for the solid phase is rather similar, with the sole difference that there is no flow on this side, hence, the convective term falls out. Thus, it can be written as

$$\rho_{\mathrm{s}}c_{\mathrm{s}}\frac{\partial T_{\mathrm{s}}}{\partial t}-\nabla\cdot\left(\kappa_{\mathrm{s}}\nabla T_{\mathrm{s}}\right)=-\dot{q}_{\mathrm{l\text{-}s}} \tag{8}$$

The two above equations must be solved by the numerical tool capable of calculating the coupled phenomena of liquid-side and solid-side behaviors, together with heat transfer in between. This is the case with OpenFOAM, however – as introduced in Section 2.2 – MSC-Marc is specialized for structural analysis of solids, together with their stress–strain calculations. In order to make the calculations solvable also by this code, we supplied it by the heat flow rates along the solid's surface, as follows.

From the calculated data of the developed velocity profile, we calculated the local heat transfer coefficients analytically. For this, the Nusselt number is needed as the first step, and for fully developed turbulent flow – as in the actual case –, it is fundamentally determined by the Dittus-Boelter correlation as follows (Winterton, 1998):

$$Nu=0.023\,Re^{0.8}\,Pr^{n} \tag{9}$$

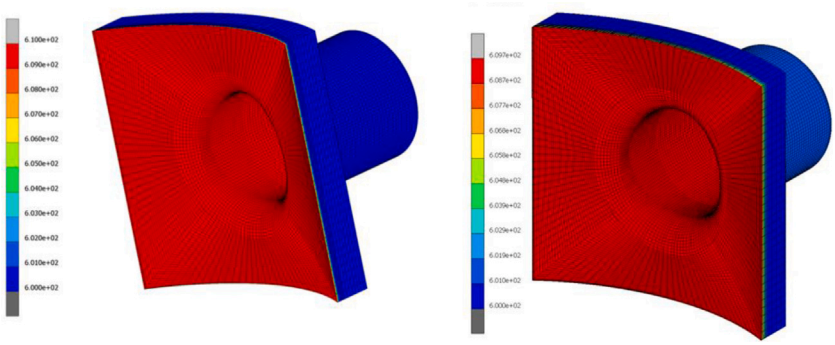

Fig. 3. Temperature profile in the investigated solid body by two basically different calculation schemes. In the case of first-type boundary condition (left), the internal surface is evidently homogeneous already at the beginning of the time evolution. In the case of third-type boundary condition (right), the heat transfer coefficient was set by the inhomogeneous flow pattern (Fig. 2), however, after a very short time (after 51 s), it also became rather homogeneous, as visible.

Table 2
Heat transfer coefficient values calculated and applied as third-type boundary condition for the FEM code.

Flow velocity (m/s)	3	4	5	6	7	8
Convective heat transfer coefficient ($W/m^2/K$)	7869	13 503	16 142	18 677	21 128	23 510

where $n = 0.4$ if the liquid is colder than the solid, and $n = 0.3$ in the opposite case.

Based on this, the effective (macroscopic) convective heat transfer coefficient can already be calculated:

$$h = \frac{Nu \cdot \kappa_l}{D_h} \tag{10}$$

by the liquid's thermal conductivity, κ_l, and the hydraulic diameter of the nozzle, D_h.

According to the results shown in Section 3.1 (Fig. 2), the flow accelerates from approximately 3 m/s to 8 m/s. Within this interval, some values of the convective heat transfer coefficients, calculated according to the analytical method, are shown in Table 2. It is to be mentioned that for 3 m/s, the characteristic size (D_h) is the internal diameter of the pressure vessel, while for higher velocities, it is that of the nozzle. Based on the values indicated in Table 2, the third-type boundary condition has been set for the nozzle model in such a way that the nozzle region has been divided into sections according to the acceleration of the flow, and in each region, the calculated convective heat transfer coefficient has been applied.

3.3. Thermal conduction

Although the critical procedure regarding thermal stresses is the uneven temperature distribution within the solid body, its description is less complicated than the previously discussed ones. Here, namely, the same energy equation can be used as for the convective heat transfer, as shown in (8), but with zero heat source ($\dot{q}_{l\text{-}s}$) on the right-hand side. We numerically solved this equation for the entire space of the nozzle corner, the results of which are graphically shown for two slightly differing outcomes in Fig. 3.

Note that the start-up of the two above calculations were two basically different schemes, the availabilities of which were outlined while describing the convective heat transfer phenomenon in Section 3.2. Accordingly, we carried out the current calculation for both first-type (Dirichlet) and third-type (Robin) boundary conditions. Based on the resulting Fig. 3, it can be seen that the differences caused by the two different methods are negligible. This is because for very high heat transfer coefficients, on the order of 10 000 $W/m^2/K$ in our case, the third-type boundary condition closely approaches the first-type one. In all similar practical cases, it is advisable to apply the simpler, hence numerically cheaper first-type boundary condition. However, we went on to calculate the induced thermal stresses along both approaches, the details of which step (in both cases) are summarized in the next subsection.

3.4. Strength of materials

The actual material behavior can be considered as isotropic and linear-thermoelastic. For this case, the basic equation of strength of materials was formulated by Eslami et al. (2015) as follows:

$$\boldsymbol{\sigma} = \frac{E}{1+\nu}\left[\boldsymbol{\varepsilon} + \frac{\nu}{1-2\nu}\varepsilon_I \boldsymbol{I}\right] - \frac{E}{1-2\nu}\alpha\left(T - T_{ref}\right)\boldsymbol{I} \tag{11}$$

where $\boldsymbol{\sigma}$ represents the stress tensor to be determined, E is the modulus of elasticity (Young's modulus), α is the thermal expansion coefficient, ν is the Poisson's ratio, $\boldsymbol{\varepsilon}$ is the strain tensor, ε_I is its first scalar invariant (the sum of elements on its main diagonal), T is the actual temperature, and T_{ref} is its reference value, while $\boldsymbol{I}$ denotes the unit tensor (the identity matrix).

By solving the characteristic equation of the resulted $\boldsymbol{\sigma}$ matrix, the three principal stresses can be determined. They are denoted as σ_1, σ_2, and σ_3, as they are arranged in descending order of their magnitudes. From them, the *von Mises stress* can be calculated as follows:

$$\sigma_{VM} = \sqrt{\frac{1}{2}\left[\left(\sigma_1 - \sigma_2\right)^2 + \left(\sigma_1 - \sigma_3\right)^2 + \left(\sigma_2 - \sigma_3\right)^2\right]} \tag{12}$$

which is a scalar quantity representing well the resulted stress at any specific points of the investigated solid body. The results of this 3D calculation are shown in Fig. 4. This picture clearly shows the critical locations in the structure with the highest stress values, which is in perfect conformance to the preceding statements (see, e.g., Dzierwa, 2016; Li et al., 2020a). The innermost points in the red zones are located at the transitional surface, and as they appear symmetrically on both the top and downsides, it is sufficient to consider only one of them throughout the upcoming calculations.

3.5. Step response function

The stress values in the critical points are investigated further, as a function of time. We set a (theoretically applied) stepwise change in the water temperature to the input of the entire series of the above outlined finite element calculations. Consequently, the resulting time function of the stress in the critical point is nothing else but the so called *step response function* ($v(t)$). This function is the one that completely characterizes any autonomous (time-invariant) dynamical systems (Burns, 2001; Ljung and Glad, 1994). Hence, the actual dynamical system identification, based on this time function, is the only duty to be done, as will be shown in the next subsection.

Because the results of the 3D numerical calculations were obtained in discrete time steps only, the points of the *step response function* are

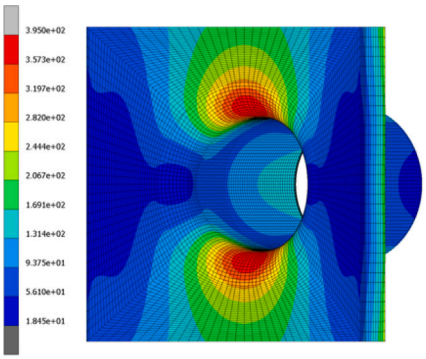

Fig. 4. Thermal stress field (von Mises stress values) within the solid body around the nozzle corner in the course of increasing the unit load. (Specifically this figure: 300 s after the stepwise excitation.).

Table 3
Characteristics of the peak thermal stress (von Mises stress) values gained by two different calculation schemes.

	Time of the peak amplitude (s)	Value of the peak amplitude (MPa)
First-type boundary condition	252	23.31
Third-type boundary condition	279	22.77

also available only in discrete time steps, as shown by the discrete points with markers in Fig. 5.

Note that we determined the discrete time series of the *step response function* along two different calculation methods, as described in Section 3.3. We compared the main characteristics of them, and we found that the differences between them are very small (Table 3). Although throughout our actual calculations we relied on the more realistic case (on applying the third-type condition), we can declare that for practical calculations, the other one (the first-type boundary condition) is fairly appropriate.

3.6. Dynamical system identification

The dynamical system in question is the one defined by the moderator temperature in the upper plenum as the *input* variable, and the von Mises thermal stress in the critical point of the nozzle corner as the *output* variable. One complete representation of any autonomous dynamical system is its *step response function*, but another one, an easier-to-use but still complete representation is the so called *transfer function*.

Dynamical identification, in this case, is to find the *transfer function*, the corresponding *step response function* of which best fits the numerically achieved discrete points. This is an optimum seeking problem, for which well-elaborated numerical tools are available. As a result of our specific and well-defined case, we got it as follows:

$$G(s) = \frac{\mathbf{\Sigma}(s)}{\mathbf{T}(s)} = -\frac{1.63 \cdot 10^{6} \cdot s^{2} + 2.41 \cdot 10^{4} \cdot s}{s^{2} + 9.28 \cdot 10^{-3} \cdot s + 4.14 \cdot 10^{-6}} \tag{13}$$

where s is the independent variable of the Laplace transform, $\mathbf{\Sigma}(s)$ is the Laplace transform of the thermal stress ($\sigma(t)$) in the critical point of the nozzle corner in MPa, and $\mathbf{T}(s)$ is the Laplace transform of the moderator temperature change ($T(t)$) in the upper plenum in K.

To evaluate the goodness of this dynamical system identification, we depicted the results of the entire 3D dynamical modeling procedure, together with the numerically fitted system in Fig. 5. As visible, the achieved and proposed (13) analytical transfer function can be considered as a well-fitting approximation of the dynamical system investigated and described in detail. As the proposed (13) transfer function is that of a linear system, and this statement also means that

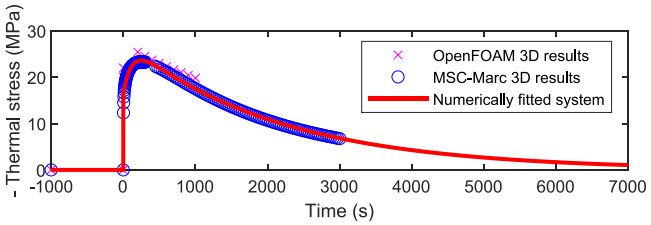

Fig. 5. Step response function fitted to the outcomes of the 3D calculations.

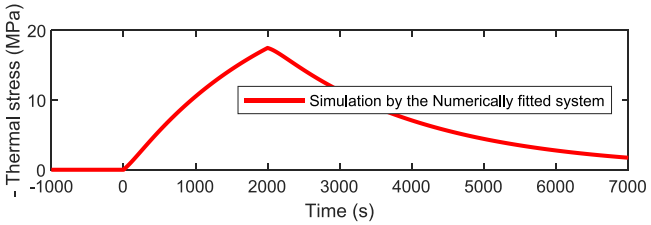

Fig. 6. The transfer function's prediction with a more realistic input scenario: the process input (the moderator temperature) changes along a linear ramp between 0 s and 2000 s.

the system in question can be well considered as a linear one. Further, this figure shows, in the same coordinate system, the results of both fundamentally differing modeling environments, the FVM-based open-source OpenFOAM, and the FEM-based commercial MSC-Marc. The results summarized in this diagram show a fair agreement not only with each other (for the same specific case), but also with several other results (reported for similar cases) by Durmaz (1980), Dzierwa (2016).

Note that the *step response function*, which is depicted in Fig. 5, is a fully descriptive, but rather theoretical representation of any dynamical system. Its input changes, namely, strictly step-like, which cannot happen in real cases. So, to demonstrate the behavior of the identified subprocess under more realistic conditions, we applied a ramp-like change to its input, the moderator temperature in the upper chamber of the RPV. The resulting output is shown in Fig. 6.

4. Final results and discussion

For balancing between maneuvering velocity and thermal stress at the most critical points, dynamical modeling of both sides is evidently needed. As dynamical models of the load control process of PWRs are generally available, a joining instationary model of the stress in the nozzle corner is necessary. This is what we developed generally and applied specifically to a relevant case.

The consecutive steps of the proposed methodology were described in the current paper, an outline and discussion of which are summarized in the subsequent paragraphs. It is to note that this procedure can be carried out for any layouts and material properties that can be numerically modeled. Because practically all nozzle designs fall definitely into this category, there is no limitation in the applicability.

First of all, each of the following steps must be considered as instationary calculations, hence, their outputs must be considered as time functions as consequences of time-dependent changes in their inputs.

Fluid dynamical description (i) of the moderator flow around the critical point (the nozzle corner) is needed to get a picture about the characteristics of the evolved flow pattern. We saw that besides a heavy increase in the flow velocity, the flow characteristics around the investigated surface are mostly turbulent.

Based on these results, in the next step, the convective heat transfer (ii) between liquid and solid must be described. To strengthen the

3D OpenFOAM results, we also applied the best available theoretical feed-forward calculation form.

The major reason for the evolution of the investigated thermal stress field within the solid body is its limited thermal conduction (iii) capability. We carried out this 3D calculation with both OpenFOAM and MSC-Marc. Here, besides applying the third-type boundary condition, we also did the MSC-Marc calculation based on the numerically cheaper first-type boundary condition. As a partial discussion, it was found that the applications of the two boundary conditions resulted in practically the same temperature fields.

The next step is to calculate the resulting 3D thermal stress field by using the theory of strength of materials (iv). The static stress fields achieved from both OpenFOAM and MSC-Marc were fully credible. Further, the resulted functions of time also confirmed that the selection between the two different boundary conditions in the previous step has only negligible effect in relation to the final outcome.

This observation indicates that in most practical applications of the proposed methodology, the accurate description of the first two steps, fluid dynamics and convective heat transfer, has a minor effect on the accuracy of the achieved dynamical model, hence, the focus should be on the remaining ones.

In the last step of the modeling procedure, the achieved time function should be turned into a description that fits well to the language of dynamical modeling and optimum control. For this, we selected the dynamical transfer function, which gives the needed relationship as function of the independent variable of the Laplace transform. This step is called dynamical system identification (v), which is practically an optimum seeking procedure for curve fitting. The best fitting result, that is, the final result of this study in our practically relevant case, is a rational fraction function (13) with two roots in both the nominator and the denominator. Visual comparison of the step response functions proves that this twice second-order linear description of the investigated subprocess is perfectly appropriate.

The main contribution of the present study is a method and its specific application to set up the dynamical model of the stress in the nozzle corner as a function of the moderator temperature, formulated in a way consistent with the terminology of control theory. Based on this, the lacking component for optimal maneuvering control became available, and, for this purpose, it can be considered as an extension to the available dynamical model of the power unit. The resulting transfer function is (13), and it is to mention that substituting it by the widely applied simple derivation of the temperature ($G(s) = s$) proves to be a very rough estimation.

Future work should target a similar dynamical thermomechanical description of the fuel rods, which seem to be the next important places of the limiting effects of maneuvering control of nuclear power plants (IAEA, 2018).

CRediT authorship contribution statement

Bálint Pudleiner: Writing – review & editing, Writing – original draft, Investigation. **Tibor Szűcs:** Writing – original draft, Investigation. **Tamás Fekete:** Writing – review & editing, Supervision. **Pal Szentannai:** Writing – review & editing, Writing – original draft, Validation, Supervision, Project administration, Methodology, Investigation, Conceptualization.

Declaration of competing interest

The authors declare that they have no known competing financial interests or personal relationships that could have appeared to influence the work reported in this paper.

Acknowledgments

The authors gratefully acknowledge the technical and in-depth help on the use of the 3D methods, especially MS-Marc, given by colleagues at HUN-REN Centre for Energy Research, Dániel Antók and Levente Tatár.

Data availability

Data will be made available on request.

References

Abdulraheem, K.K., Korolev, S.A., 2021. Robust optimal-integral sliding mode control for a pressurized water nuclear reactor in load following mode of operation. Ann. Nucl. Energy 158, 108288. http://dx.doi.org/10.1016/j.anucene.2021.108288, URL https://www.sciencedirect.com/science/article/pii/S030645492100164X.

Ayhan, H., Ergün, S., 2013. Modeling VVER-1200 reactor pressure vessel by using computational fluid dynamics tools. In: International Conference "Nuclear Power for the People. URL https://www.academia.edu/download/42701253/Modeling_VVER-1200_Reactor_Pressure_Vess20160215-15389-w0ei3n.pdf.

Belkhir, F., Cabo, D.K., Feigner, F., Frey, G., 2015. Optimal startup control of a steam power plant using the jmodelica platform. IFAC-PapersOnLine 48 (1), 204–209. http://dx.doi.org/10.1016/j.ifacol.2015.05.050, URL http://www.sciencedirect.com/science/article/pii/S2405896315000518.

Burns, R.S., 2001. Advanced Control Engineering. URL https://shop.elsevier.com/books/advanced-control-engineering/burns/978-0-7506-5100-4.

Chaudhry, V., Kumar, A., Ingole, S.M., Balasubramanian, A.K., Muktibodh, U.C., 2014. Thermo-mechanical transient analysis of reactor pressure vessel. Procedia Eng. 86, 809–817. http://dx.doi.org/10.1016/j.proeng.2014.11.101, URL https://www.sciencedirect.com/science/article/pii/S1877705814020608.

Cheng, Y., Huang, M., Li, Y., Liu, W., Wang, B., Meng, X., Ouyang, X., 2023. Influence of interaction among multiple cracks on crack propagation in nozzle corner of reactor pressure vessel. Ann. Nucl. Energy 194, 110142. http://dx.doi.org/10.1016/j.anucene.2023.110142, URL https://www.sciencedirect.com/science/article/pii/S0306454923004619.

Durmaz, A., 1980. Dynamic behaviour of material states in steam power plant control. Automatica 16 (1), 45–52. http://dx.doi.org/10.1016/0005-1098(80)90085-0, URL https://www.sciencedirect.com/science/article/pii/0005109880900850.

Dzierwa, P., 2016. Optimum heating of pressure components of steam boilers with regard to thermal stresses. J. Therm. Stresses 39 (7), 874–886. http://dx.doi.org/10.1080/01495739.2016.1189773, WOS:000378629200007.

Dzierwa, P., Taler, D., Taler, J., Trojan, M., 2014. Optimum Heating of Thick Wall Pressure Components of Steam Boilers. Amer Soc Mechanical Engineers, New York, WOS:000361161600019.

Elsisi, M., Abdelfattah, H., 2020. New design of variable structure control based on lightning search algorithm for nuclear reactor power system considering load-following operation. Nucl. Eng. Technol. 52 (3), 544–551. http://dx.doi.org/10.1016/j.net.2019.08.003, Num Pages: 8 Place: Daejeon Publisher: Korean Nuclear Soc Web of Science ID: WOS:000516803800010.

EN12952-3, 2021. EN 12952-3:2021-08 - Water-Tube Boilers and Auxiliary Installations - Part 3: Design and Calculation for Pressure Parts of the Boiler. Technical Report, Beuth Verlag GmbH, http://dx.doi.org/10.31030/3238498, URL https://www.beuth.de/de/-/-/335107104.

Eslami, M.R., Hetnarski, R.B., Ignaczak, J., Noda, N., Sumi, N., Tanigawa, Y., 2015. Theory of Elasticity and Thermal Stresses: Explanations, Problems and Solutions, 2013th edition Springer.

Greenshields, C.J., Weller, H.G., 2022. Notes on Computational Fluid Dynamics: General Principles. CFD Direct Limited, Reading, UK, URL https://cfd.direct/openfoam/cfd-book/.

Grunwald, R., Caviezel, C., 2017. Load-Following Capability of German Nuclear Power Plants. Summary. http://dx.doi.org/10.5445/IR/1000137922, URL https://publikationen.bibliothek.kit.edu/1000137922/130083404.

Hu, X., Zhou, T., Li, C., Zhang, M., Zhu, S., Yang, H., 2024. Investigation on the dynamic characteristics under load regulation in CFB boiler with whole loop model. Chem. Eng. Sci. 287, 119784. http://dx.doi.org/10.1016/j.ces.2024.119784, URL https://www.sciencedirect.com/science/article/pii/S0009250924000848.

IAEA, 2018. Non-baseload Operation in Nuclear Power Plants: Load Following and Frequency Control Modes of Flexible Operation. International Atomic Energy Agency, URL https://www-pub.iaea.org/MTCD/Publications/PDF/P1756_web.pdf.

Jeong, S.H., Chung, K.S., Ma, W.J., Yang, J.S., Choi, J.B., Kim, M.K., 2022. Thermal stress intensity factor solutions for reactor pressure vessel nozzles. Nucl. Eng. Technol. 54 (6), 2188–2197. http://dx.doi.org/10.1016/j.net.2022.01.006, URL https://www.webofscience.com/wos/woscc/full-record/WOS:000822928600013. Num Pages: 10 Place: Daejeon Publisher: Korean Nuclear Soc Web of Science ID: WOS:000822928600013.

Jin, T., He, Z., Liu, P., Wang, Z., Li, Y., Wang, D., 2021. A new stress intensity factor solution based on the response surface method for nozzle corner cracks in nuclear reactor for thermal energy generation. Front. Energy Res. 9, URL https://www.frontiersin.org/articles/10.3389/fenrg.2021.801919.

Kondryakov, E.O., Kharchenko, V.V., 2024. Application of modern approaches to the numerical modeling of the stress-strain state for the strength assessment of complex units of the NPP primary circuit equipment. part 3. application of submodeling technique and extended finite element method for calculation of the reactor pressure vessel nozzle zone. Strength Mater. 56 (3), 467–476. http://dx.doi.org/10.1007/s11223-024-00662-4.

Lemaître, J., Chaboche, J.-L., 2005. Mechanics of Solid Materials, Revised ed. edition Cambridge University Press, Cambridge, URL https://www.amazon.com.be/-/en/Jean-Lema%C3%AEtre/dp/0521477581?language=en_GB.

Li, M., Benaarbia, A., Morris, A., Sun, W., 2020a. Assessment of potential service-life performance for MarBN steel power plant header under flexible thermomechanical operations. Int. J. Fatigue 135, 105565. http://dx.doi.org/10.1016/j.ijfatigue.2020.105565, URL https://www.webofscience.com/wos/woscc/full-record/WOS:000525299400035. Place: Oxford Publisher: Elsevier Sci Ltd WOS:000525299400035.

Li, Y., Jin, T., Wang, Z., Wang, D., 2020b. Engineering critical assessment of RPV with nozzle corner cracks under pressurized thermal shocks. Nucl. Eng. Technol. 52 (11), 2638–2651. http://dx.doi.org/10.1016/j.net.2020.04.019, URL https://www.sciencedirect.com/science/article/pii/S1738573320300012.

Liu, K., Huang, M., Lin, J., Jiang, H., Wang, B., Matsuda, H., 2020. The effects of thermal stress on the crack propagation in AP1000 reactor pressure vessel. Theor. Appl. Fract. Mech. 110, 102798. http://dx.doi.org/10.1016/j.tafmec.2020.102798, URL https://www.sciencedirect.com/science/article/pii/S0167844220303748.

Liu, R., Huang, M., Peng, Y., Wen, H., Huang, J., Ruan, C., Ma, H., Li, Q., 2018. Analysis for crack growth regularities in the nozzle-cylinder intersection area of reactor pressure vessel. Ann. Nucl. Energy 112, 779–793. http://dx.doi.org/10.1016/j.anucene.2017.10.021, URL https://www.sciencedirect.com/science/article/pii/S0306454916309835.

Liu, C., Jiao, G.c., Chandwani, R., Timbrell, C., 2021. Study on application range of SIF calculation method for nozzle corner crack in pressure vessel for ASME XI code. Int. J. Press. Vessels Pip. 193, 104478. http://dx.doi.org/10.1016/j.ijpvp.2021.104478, URL https://www.sciencedirect.com/science/article/pii/S0308016121001733.

Ljung, L., 1998. System Identification: Theory for the User, second ed. Pearson, Upper Saddle River, NJ.

Ljung, L., 2024. System Identification Toolbox User's Guide. Release 2024b. The MathWorks, Inc, Natick, Massachusetts, United States, URL https://www.mathworks.com/help/pdf_doc/ident/ident_ug.pdf.

Ljung, L., Glad, T., 1994. Modeling of Dynamic Systems, first ed. Pearson, Englewood Cliffs, N.J.

Ludwig, H., Salnikova, T., Stockman, A., Waas, U., 2010. Load cycling capabilities of German nuclear power plants (NPP). URL https://www.semanticscholar.org/paper/Load-cycling-capabilities-of-German-Nuclear-Power-Ludwig-Salnikova/7c830f630e164047162709221962f48ba2689a31.

Marusic, A., Loncar, D., Batelic, J., Frankovic, V., 2016. Increasing flexibility of coal power plant by control system modifications. Therm. Sci. 20 (4), 1161–1169. http://dx.doi.org/10.2298/TSCI160314159M, URL https://www.webofscience.com/wos/woscc/full-record/WOS:000382511600013. Conference Name: 10th Conference on Sustainable Development of Energy, Water and Environment Systems (SDEWES) Num Pages: 9 Place: Belgrade Publisher: Vinca Inst Nuclear Sci Web of Science ID: WOS:000382511600013.

Miedlar, P., Berens, A.P., Gunderson, A., Gallagher, J., 2002. Analysis and support initiative for structural technology (ASIST) delivery order 0016: USAf damage tolerant design handbook: Guidelines for the analysis and design of damage tolerant aircraft structures. URL https://www.semanticscholar.org/paper/Analysis-and-Support-Initiative-for-Structural-USAF-Miedlar-Berens/c7826a425b66560d2f910372bc68b5bf03d9fb48.

Mohanty, S., Soppet, W.K., Majumdar, S., Natesan, K., 2016. Thermal–mechanical stress analysis of pressurized water reactor pressure vessel with/without a preexisting crack under grid load following conditions. Nucl. Eng. Des. 310, 112–124. http://dx.doi.org/10.1016/j.nucengdes.2016.09.020, URL https://www.sciencedirect.com/science/article/pii/S0029549316303387.

Mousakazemi, S.M.H., 2021. Comparison of the error-integral performance indexes in a GA-tuned PID controlling system of a PWR-type nuclear reactor point-kinetics model. Prog. Nucl. Energy 132, 103604. http://dx.doi.org/10.1016/j.pnucene.2020.103604, Num Pages: 9 Place: Oxford Publisher: Pergamon-Elsevier Science Ltd Web of Science ID: WOS:000613917800005.

Naweed, M., Murtaza, U.T., Siddique, W., 2023. Fracture mechanics analysis of a closure head of a PWR reactor pressure vessel the effect of bolt pre-load and thermal stresses. Ann. Nucl. Energy 189, 109843. http://dx.doi.org/10.1016/j.anucene.2023.109843, URL https://www.sciencedirect.com/science/article/pii/S0306454923001627.

Ochsner, A., Ochsner, M., 2018. A First Introduction to the Finite Element Analysis Program MSC Marc/Mentat, Softcover reprint of the original 2nd ed. 2018 edition Springer, URL https://link.springer.com/book/10.1007/978-3-319-71915-3.

Oh, C., Lee, S., Jhung, M.J., 2022. Analytical method to estimate cross-section stress profiles for reactor vessel nozzle corners under internal pressure. Nucl. Eng. Technol. 54 (1), 401–413. http://dx.doi.org/10.1016/j.net.2021.08.001, URL https://www.sciencedirect.com/science/article/pii/S1738573321004873.

Park, J., Kim, T., Seong, S., Koo, S., 2022. Control automation in the heat-up mode of a nuclear power plant using reinforcement learning. Prog. Nucl. Energy 145, 104107. http://dx.doi.org/10.1016/j.pnucene.2021.104107, Num Pages: 10 Place: Oxford Publisher: Pergamon-Elsevier Science Ltd Web of Science ID: WOS:000751707200006.

Rabazzi, S.M., Albanesi, A.E., Nervi, J.E.R., Signorelli, J.W., 2024. Highly detailed structural integrity assessment of the reactor pressure vessel nozzle of Atucha-I during a pressurized thermal shock event. Nucl. Eng. Des. 418, 112905. http://dx.doi.org/10.1016/j.nucengdes.2024.112905, URL https://www.sciencedirect.com/science/article/pii/S0029549324000074.

Rabie, M.A., Elshahat, A.E., Hassan, M.H., 2024. Control oriented modeling of VVER-1200 using modelica. Nucl. Eng. Des. 420, 112980. http://dx.doi.org/10.1016/j.nucengdes.2024.112980, URL https://www.sciencedirect.com/science/article/pii/S0029549324000827.

Raskovic, P.O., Cvetanovic, G., Vujanovic, M., Daniel, R.S., Guzovic, Z., Duic, N., Oka, S.N., 2022. The progress toward more sustainable energy, water and environmental systems – approaches and applications. Therm. Sci. 26 (5), 4057–4066. http://dx.doi.org/10.2298/TSCI2205057R, URL https://www.webofscience.com/wos/woscc/full-record/WOS:000908401500001. Num Pages: 10 Patent Number: B Place: Belgrade Publisher: Vinca Inst Nuclear Sci Web of Science ID: WOS:000908401500001.

Ray, Wu, M.K., Carpino, M., Lorenzo, C.F., 1994. Damage-mitigating control of mechanical systems: Part I – conceptual development and model formulation. In: American Control Conference. Publ by IEEE, pp. 1172–1176. http://dx.doi.org/10.23919/acc.1993.4793051, URL https://pennstate.pure.elsevier.com/en/publications/damage-mitigating-control-of-mechanical-systems-part-i-conceptual-2.

Rodriguez-Reyes, V.I., Abundez-Pliego, A., Petatan-Bahena, K.E., Miranda-Acatitlan, K.R., Colin-Ocampo, J., Blanco-Ortega, A., 2024. Comparative evaluation of fatigue life estimation under variable amplitude loading through damage models based on entropy. Fatigue Fract. Eng. Mater. Struct. 47 (5), 1584–1601. http://dx.doi.org/10.1111/ffe.14262, URL https://www.webofscience.com/wos/woscc/full-record/WOS:001160910400001. Num Pages: 18 Place: Hoboken Publisher: Wiley Web of Science ID: WOS:001160910400001.

Rusin, A., Nowak, G., Łukowicz, H., Kosman, W., Chmielniak, T., Kaczorowski, M., 2021. Selecting optimal conditions for the turbine warm and hot start-up. Energy 214, 118836. http://dx.doi.org/10.1016/j.energy.2020.118836, URL https://www.sciencedirect.com/science/article/pii/S0360544220319435.

Salman, A.E., Gomaa, H.E., 2025. A boron concentration maneuvering control algorithm for reactivity management during transients in VVER-1000 nuclear power units. Ann. Nucl. Energy 218, 111381. http://dx.doi.org/10.1016/j.anucene.2025.111381, URL https://www.sciencedirect.com/science/article/pii/S0306454925001987.

Santucci, S., Vanel, L., Ciliberto, S., 2007. Slow crack growth: Models and experiments. Eur. Phys. Journal-Special Top. 146, 341–356. http://dx.doi.org/10.1140/epjst/e2007-00192-9, URL https://www.webofscience.com/wos/woscc/full-record/WOS:000247812800030. Num Pages: 16 Place: Heidelberg Publisher: Springer Heidelberg Web of Science ID: WOS:000247812800030.

Sharabi, M., González-Albuixech, V.F., Lafferty, N., Niceno, B., Niffenegger, M., 2016. Computational fluid dynamics study of pressurized thermal shock phenomena in the reactor pressure vessel. CFD4NRS-5, Nucl. Eng. Des. CFD4NRS-5, 299, 136–145. http://dx.doi.org/10.1016/j.nucengdes.2015.10.014.URL https://www.sciencedirect.com/science/article/pii/S0029549315004665,

Sun, A., Pu, S., He, Z., Xiao, K., Sun, P., Wang, P., Wei, X., 2021. Application of model free active disturbance rejection controller in nuclear reactor power control. Prog. Nucl. Energy 140, 103907. http://dx.doi.org/10.1016/j.pnucene.2021.103907, Num Pages: 11 Place: Oxford Publisher: Pergamon-Elsevier Science Ltd Web of Science ID: WOS:000709543600003.

Szentannai, P., Fekete, T., 2022. Integrated optimization of process control and its effect on structural integrity – A systematic review. Eng. Fail. Anal. 106101. http://dx.doi.org/10.1016/j.engfailanal.2022.106101, URL https://www.sciencedirect.com/science/article/pii/S1350630722000759.

Szentannai, P., Fekete, T., 2025. Life-time considering control (LTCC) of load changes in nuclear and conventional power plants for reducing ecological footprint. In: Lackner, M., Sajjadi, B., Chen, W.-Y. (Eds.), Handbook of Climate Change Mitigation and Adaptation. Springer, New York, NY, pp. 1–69. http://dx.doi.org/10.1007/978-1-4614-6431-0_172-3.

Trampus, P., 2024. Materials challenges of the new nuclear power plant in Hungary. Period. Polytech. Mech. Eng. 68 (4), 328–335. http://dx.doi.org/10.3311/PPme.37668, URL https://pp.bme.hu/me/article/view/37668. Number: 4.

Vajpayee, V., Becerra, V., Bausch, N., Deng, J., Shimjith, S.R., Arul, A.J., 2020. Dynamic modelling, simulation, and control design of a pressurized water-type nuclear power plant. Nucl. Eng. Des. 370, 110901. http://dx.doi.org/10.1016/j.nucengdes.2020.

110901, Num Pages: 22 Place: Lausanne Publisher: Elsevier Science Sa Web of Science ID: WOS:000598959900007.

Vajpayee, V., Becerra, V., Bausch, N., Deng, J., Shimjith, S.R., Arul, A.J., 2021. L-1-adaptive robust control design for a pressurized water-type nuclear power plant. Ieee Trans. Nucl. Sci. 68 (7), 1381–1398. http://dx.doi.org/10.1109/TNS.2021.3090526, URL https://www.webofscience.com/wos/woscc/full-record/WOS:000675432600003. Place: Piscataway Publisher: Ieee-Inst Electrical Electronics Engineers Inc WOS:000675432600003.

Wang, S., Wang, B., Wu, G., Xue, H., Sun, Y., Zhu, J., 2023. Effects of angles and shapes of a corner crack on the driving force at a set-in nozzle-cylinder in a PWR pressure vessel. Ann. Nucl. Energy 192, 109991. http://dx.doi.org/10.1016/j.anucene.2023.109991, URL https://www.sciencedirect.com/science/article/pii/S0306454923003109.

Winterton, R.H.S., 1998. Where did the Dittus and Boelter equation come from? Int. J. Heat Mass Transfer 41 (4), 809–810. http://dx.doi.org/10.1016/S0017-9310(97)00177-4, URL https://www.sciencedirect.com/science/article/pii/S0017931097001774.

Zeng, W., Jiang, Q., Liu, Y., Yan, S., Zhang, G., Yu, T., Xie, J., 2021. Core power control of a space nuclear reactor based on a nonlinear model and fuzzy-PID controller. Prog. Nucl. Energy 132, 103564. http://dx.doi.org/10.1016/j.pnucene.2020.103564, Num Pages: 11 Place: Oxford Publisher: Pergamon-Elsevier Science Ltd Web of Science ID: WOS:000613916500005.

Zhou, G., Tan, D., 2023. Review of nuclear power plant control research: Neural network-based methods. Ann. Nucl. Energy 181, 109513. http://dx.doi.org/10.1016/j.anucene.2022.109513, Num Pages: 15 Place: Oxford Publisher: Pergamon-Elsevier Science Ltd Web of Science ID: WOS:000878994800005.